electronics

MDPI

Article

Dynamic Characteristic Analysis of Multi-Virtual Synchronous Generator Systems Considering Line Impedance in Multi-Node Microgrid

Wei Xie [1], Liangzi Li [1], Weihao Kong [1], Zheng Peng [1], Xiaogang Li [1], Dandan Jiao [1], Chenyi Xu [2,*] and Zebin Yang [2]

[1] Henan Jiuyu Enpai Power Technol Co., Ltd., Zhengzhou 450052, China; xnyjcz@163.com (W.X.); chengzi_llz@sina.com (L.L.); kongweihao1996@hotmail.com (W.K.); 18240585107@163.com (Z.P.); lxg622@163.com (X.L.); 13939069667@163.com (D.J.)

[2] State Key Laboratory of Electrical Insulation and Power Equipment, Xi'an 710045, China; yangzbin@xjtu.edu.cn

* Correspondence: 1471608065@stu.xjtu.edu.cn

Abstract: With the increasing integration of distributed energy resources into modern power systems, virtual synchronous generators (VSGs) have been a promising approach to imitate the inertial response of synchronous generators, thereby enhancing microgrid stability in a dynamic state. When many VSGs are integrated into microgrids, the dynamic characteristics of the system become increasingly complex. Current studies typically assume that different VSGs are connected to a common coupling point, focusing on analyzing the interaction characteristics, which may overlook the widely distributed line impedances in microgrids with distance between different facilities. This may lead to incomplete understanding of the interaction dynamics when VSGs are distributed over long feeder lines. Therefore, this paper proposes and investigates a multi-node, multi-VSG model incorporating line impedances among different nodes, establishing transfer function models for multi-node load disturbances and the frequency responses of individual VSGs. The study explores the dynamic response characteristics of VSGs under varying parameter influences and proposes principles for designing VSG port impedance and inertia parameters to optimize system dynamic frequency characteristics. The findings, validated through simulations in PSCAD v46, provide insights for enhancing the flexibility and reliability of grids incorporating VSGs.

Keywords: VSG; multi-node; dynamic frequency characteristic; microgrids; frequency regulation

Citation: Xie, W.; Li, L.; Kong, W.; Peng, Z.; Li, X.; Jiao, D.; Xu, C.; Yang, Z. Dynamic Characteristic Analysis of Multi-Virtual Synchronous Generator Systems Considering Line Impedance in Multi-Node Microgrid. *Electronics* **2024**, *13*, 4649. https://doi.org/10.3390/electronics13234649

Academic Editor: Pablo García Triviño

Received: 6 October 2024
Revised: 13 November 2024
Accepted: 20 November 2024
Published: 25 November 2024

1. Introduction

Grid-connected inverters are essential for linking renewable energy sources and energy storage with the microgrid [1–4]. However, with the increased installation of distributed power sources, the reduction in synchronous generators leads to decreased system inertia and increased voltage fluctuations [5–7].

The Grid-Following (GFL) control strategy, as the mainstream inverter control strategy currently applied in power grids, has been successfully utilized for the grid connection of renewable energy sources [2,8]. GFL control utilizes a phase-locked loop (PLL) to track the phase angle of the grid voltage [3,9]. This synchronization method allows for rapid dynamic adjustment of the output current, which enhances grid flexibility and optimizes the use of renewable resources such as wind and solar power [4]. Nonetheless, in the weak grid, the synchronization loop may have problems in stability, leading to potential disconnection of inverters [10]. Additionally, when grid power is mainly supplied by inverters using GFL control, the lack of inertia can cause substantial frequency deviations due to changes in generation or load, resulting in system instability [8]. Therefore, as grid stability continues to weaken, strategies like the virtual synchronous generator (VSG), which provide voltage/frequency support and improved power regulation [3], become increasingly valuable. These strategies can provide relatively stable voltage and frequency when facing disturbance from both the source and load sides [11].

The VSG control method is designed based on the mechanical equations of a synchronous generator (SG) to develop an active power control loop, thereby establishing frequency and phase references [5,12]. To adapt the VSG control to many different situations, including filter type, sensor type and location, and dc-link power source type, many different VSG methods are proposed [13–15]. The critical parts of them include active and reactive power control, which relate to the frequency and voltage control, respectively [16,17]. By controlling the power of energy storage on the inverter's dc side, the VSG provides rotational kinetic energy to simulate the inertia of SG, offering damping and inertia after frequency variations. Moreover, reactive power control, like virtual excitation control or direct reactive power droop control [5], is investigated for optimizing control strategies to enhance voltage performance in the dynamic state [6].

Correspondingly, the performance of VSGs in microgrids is investigated in many studies. Usually, single-machine systems are analyzed in which a single VSG connects to a voltage source in series with line impedance. In these studies, small-signal models have been developed for a single-VSG system, and frequency domain analysis is used to explore the stability boundaries considering virtual inertia and other control parameters [18–20]. However, the conclusion of single-VSG analysis neglects the interaction among different inverters, which may not be used in situations with multiple distributed sources, and the related dynamic performance is not considered [21]. Therefore, some researchers study the interaction among different VSGs, where stability issues and transient behaviors are studied under various conditions. In [22], a method based on the Lyapunov method is proposed to control the oscillations of VSGs around the grid's center-of-inertia frequency. In [23], a state-space model of two VSGs is developed to analyze the stability and dynamic performance. In [24], a master–slave control method with instantaneous frequency is proposed in islanded microgrids. In summary, this research focuses on the stability of multiple VSGs in parallel at a Point of Common Coupling (PCC), either in an islanded or a grid-connected microgrid. These studies do not fully consider the dynamic interaction and the frequency response features.

Usually, the line impedance between different nodes is simplified and not considered [25]. The interactions between multiple VSG units introduce further complexity, particularly when connected across different nodes. In [26], a parameter-adaptive VSG controller for multi-terminal direct-current systems is proposed to improve the damping of the low-frequency oscillation problem and mitigate the impact of VSGs on dc voltage stability. In [27,28], a transfer function model of VSGs is proposed to analyze the frequency and phase response of an ac bus. Interactive frequency performance is improved with VSG control methods. However, this paper also uses the PCC to describe the interaction among different inverters, without considering the impedance among different nodes. Moreover, in the following study [29], this model is further developed to describe the power interaction with the same weakness. Some papers consider virtual damping in improving the dynamic performance. In [30], the influence of damping is analyzed after considering changing of the reference, where the transient power is also studied. Other studies may consider impedance in relation to both resistance and inductance. For example, in both [25,30], the resistance in line impedance is considered for performance analysis. However, in all of these studies, they use the PCC as a base and all converters connect to the PCC. Simulation-based analysis is also considered in some studies. This technology is usually applied to power grids, which mainly focus on specific configurations. While simulations serve as a valuable analytical tool, their inherent constraints highlight the need for mathematical modeling to enhance the understanding of multi-VSG dynamics. Therefore, in the situation that the line is long and the impedance between different nodes cannot be neglected, the performance may not be precise enough. It is necessary to develop models that incorporate the influence of line impedance between different nodes to better determine the performance of VSG-based systems.

This paper investigates the influence of line impedance parameters between different nodes and load disturbances with various spatial distributions on the configuration of inertia and port impedance in multi-VSG parallel systems under a multi-node network topology. The dynamic characteristics are analyzed using a transfer function model and validated through simulation results. This study provides insights for improving the frequency dynamic characteristics of multi-VSG systems, aiming to enhance frequency stability, flexibility, and reliability in distribution networks, especially in systems where VSGs are widely dispersed. The main contributions of this paper are summarized as follows:

(1) A parallel model of multi-VSGs is proposed. Compared with existing models, this model considers that the VSGs are not connected to a PCC, where the line impedance between different nodes is considered.
(2) With the proposed model, different parameters of VSGs from the front node to end node are considered. Therefore, the VSG's parameters in different locations can be further studied to improve the transient performance, which was often neglected in previous research.
(3) In the parameter analysis, both the inertia and impedance are considered in many different scenarios, which can provide a substantial reference for choosing reasonable parameters whilst considering the location of VSGs.

2. VSG Control Strategies and Dynamic Characteristic Analysis

2.1. The Principle of the VSG Control Strategy

In a typical weak grid, considering factors such as LCL-type filter impedance, inverter virtual impedance, and transformer equivalent impedance, the AC port characteristics of inverters are nearly inductive. Therefore, the phase difference is related to the active power among different nodes, where the *P-f* droop characteristic is adopted to realize frequency and active power regulation. The active power control strategy employed in this paper for a VSG is centered around the rotor mechanical equations and frequency control equations of synchronous generators. The relationship between torque and power is illustrated in Equation (1). Here, T_m represents the mechanical torque and T_e represents the electromagnetic torque. In this paper, T_m in a VSG is determined by the droop control loop, which is illustrated in Equation (2), replacing the traditional governor control loop for primary frequency regulation and simplifying the control loop.

$$J\frac{\mathrm{d}\omega}{\mathrm{d}t}=T_{\mathrm{m}}-T_{\mathrm{e}}-D_{\mathrm{p}}(\omega-\omega_{\mathrm{g}}) \quad (1)$$

where J is the rotational inertia; D_p is the damping coefficient; ω is the synchronous machine rotational frequency; ω_g is frequency at the grid connection point.

$$T_{\mathrm{m}}=\frac{P_{\mathrm{ref}}+k_{\mathrm{p}}(\omega_{\mathrm{ref}}\text{-}\omega)}{\omega}\approx\frac{P_{\mathrm{ref}}+k_{\mathrm{p}}(\omega_{\mathrm{ref}}\text{-}\omega)}{\omega_0} \quad (2)$$

where k_P is the droop coefficient; ω_{ref} and P_{ref} are the reference of frequency and power; ω is the actual frequency in a VSG. For analytical convenience, the rated frequency ω_0 is used in Equation (2) to replace the actual frequency in the power and torque relationship.

By combining Equations (1) and (2) and neglecting the effect of the damping coefficient, we obtain Equation (3).

$$J\omega_0\frac{\mathrm{d}\omega}{\mathrm{d}t}=P_{\mathrm{ref}}-P_{\mathrm{out}}+k_{\mathrm{P}}(\omega_{\mathrm{ref}}-\omega) \quad (3)$$

2.2. The Complete VSG Control Strategy

With the analysis, the diagram of the complete control loop of VSG is shown in Figure 1. The active power control of a VSG is from Equations (1) and (3). The reactive power loop of the VSG is same as the regular Q-V droop control. In addition, the inner dual loop control is applied, which includes both the voltage and current control loops with a PI regulator.

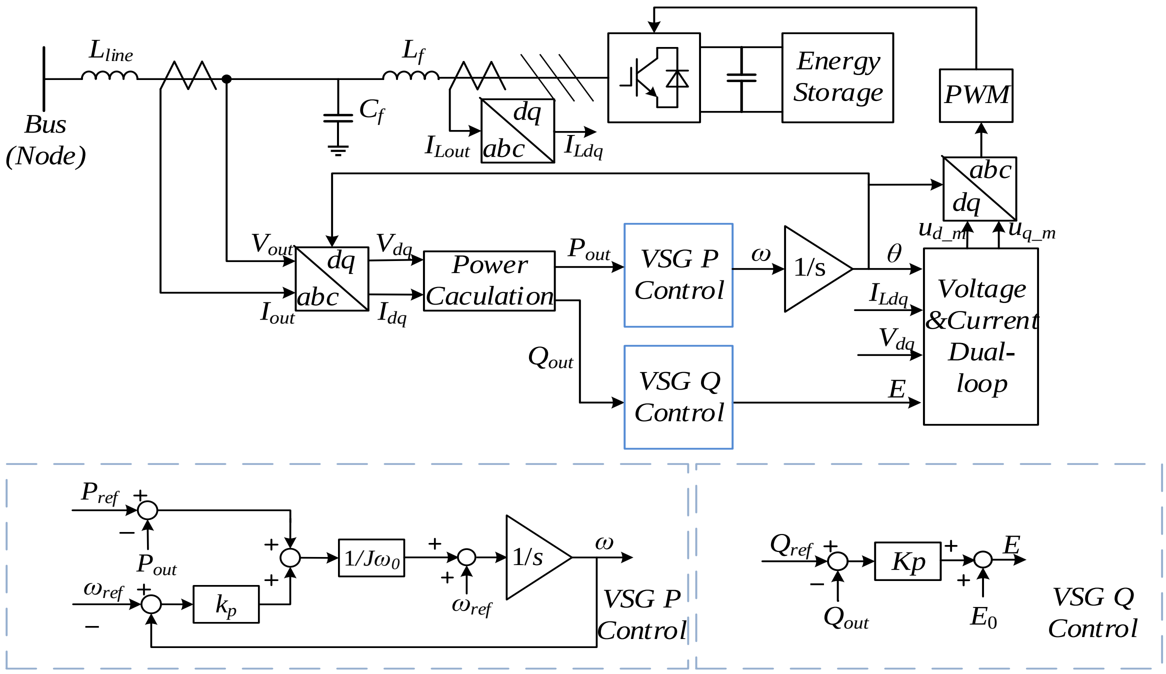

Figure 1. The diagram of complete VSG control strategy.

2.3. Dynamic Characteristic Analysis of Single Grid-Connected VSG

To analyze the impact of the frequency dynamics of the VSG control strategy on load power disturbance, we consider the case of a single grid-connected VSG operating in parallel with a load. Ignoring the frequency characteristics of the load and line losses, when the load changes, the power should be balanced among the grid, VSG and load, which is shown in (4).

$$\Delta P_g + \Delta P_{\text{vsg}} = \Delta P_{\text{load}} \tag{4}$$

We extract the relationship between frequency variation and power variation and perform the Laplace transform in Equation (3), which allows us to assess the impact of changes in inverter output power on the variation in inverter output frequency, as shown in Equation (5). The equation indicates that changes in inverter output power affect the deviation of the steady-state frequency. Adjusting the inertia influences the transient frequency variation.

$$\Delta\omega_{\text{vsg}} = -\frac{\Delta P_{\text{vsg}}}{J\omega_0 s + k_{\text{p}}} \tag{5}$$

When the output port of the VSG is predominantly inductive with reactance X_L, the relationship between active power and phase can be expressed as Equation (6). This expression is one of the theoretical foundations for frequency control in a VSG.

$$\Delta P_{\text{vsg}} = \frac{3EU_{\text{s}}}{2X_{\text{L}}}\Delta\delta = k_{\text{vsg}}(\Delta\theta_{vsg} - \Delta\theta_1) \tag{6}$$

where E is the equivalent electromotive force at the output port of the VSG; U_s is the voltage at the node; k_{vsg} is the line coefficient under the assumption of there being no voltage magnitude variation, which equals $3EU_s/2X_L$; θ_1 is the voltage phase at the node.

Similarly, for the power grid, a similar relationship between active power output and phase angle is shown in Equation (7).

$$\Delta P_{\mathrm{g}} = \frac{3U_g U_{\mathrm{s}}}{2X_{\mathrm{g}}}\Delta\delta_g = k_{\mathrm{g}}(\Delta\theta_g - \Delta\theta_1) \tag{7}$$

where U_g is the voltage at the grid, k_g is the line coefficient under the assumption of minus voltage magnitude variation, and θ_g is the voltage phase at the grid. Here, the grid phase is set as the reference axis of phase.

Combining Equations (4)–(7), for a single grid-connected VSG operating in parallel with a load, the impact of load power variation on the phase of the bus is given by Equation (8). It can be observed that a change in load power causes an instantaneous phase shift at the bus, and the subsequent frequency variation is influenced by the rotational inertia and the impedance of the VSG's output port.

$$\frac{\Delta\theta_1}{\Delta P_{\mathrm{Load}}} = -\frac{J\omega_0 s^2 + k_{\mathrm{p}}s + k_{\mathrm{d}}}{(k_{\mathrm{d}} + k_g)(J\omega_0 s^2 + k_{\mathrm{p}}s) + k_{\mathrm{d}}k_g} \tag{8}$$

It can also be observed that the VSG emulates the inertia characteristics of synchronous generators, improving the dynamic frequency response of the grid, reducing the rate of change in frequency, and providing inertial support for the grid frequency. This paper further develops the models with the impact of line impedance between different nodes, thereby enhancing the frequency performance analysis for multiple VSGs in microgrids.

3. Analysis and Modeling of Multi-VSG Parallel Systems

In a multi-VSG parallel system with a PCC, all inverters deliver power to the same node. This section uses a three-machine system as an example to establish the mathematical models for both the single-node multi-machine parallel topology with a common coupling point and the multi-node multi-machine parallel topology. Based on these models, a comparative analysis is performed to investigate the impact of line impedances between nodes on the system's frequency response.

3.1. Transfer Function Model of a Single-Node Multi-Machine Grid-Connected System

Firstly, by further developing a model based on the model in Section 2 into a dual-machine system, the transfer function for the node frequency response can be easily obtained. After the load changes, the voltage phase at the node will experience a sudden shift, and the subsequent frequency variation will be influenced by the rotational inertia set for both VSGs (J_1 and J_2) and the magnitude of the droop coefficient.

$$\frac{\Delta\theta_1}{\Delta P_{\mathrm{load}}} = -\left(\frac{1}{k_g + \dfrac{1}{\dfrac{1}{k_{\mathrm{d1}}} + \dfrac{1}{J_1\omega_0 s^2 + k_{\mathrm{p1}}s}} + \dfrac{1}{\dfrac{1}{k_{\mathrm{d2}}} + \dfrac{1}{J_2\omega_0 s^2 + k_{\mathrm{p2}}s}}}\right) \tag{9}$$

By comparing the forms of Equations (8) and (9), the phase deviation at the connected node caused by a load step change for each VSG can be described by a similar expression in a single-node multi-machine system. The expression can also be derived from Equations (5) and (6), as shown in Equation (10). This expression is defined as the additional active power compensation provided by the VSG when a load step occurs at the connected node, denoted in this paper as $k_m(s)$, which equals $\Delta P_{vsg\_i}/\Delta\theta_1$.

$$k_{\mathrm{m}}(s)=\frac{1}{\dfrac{1}{k_{\mathrm{d}}}+\dfrac{1}{J\omega_0 s^2+k_{\mathrm{p}}s}} \tag{10}$$

At this point, the single-node two-VSG system and extended single-node n-VSG grid-connected systems corresponding to Equations (8) and (9) can all be represented by a single expression, as shown in Equation (11). For the single-node three-VSG system in Figure 2, n = 3 in Equation (11).

$$\frac{\Delta\theta_1}{\Delta P_{\mathrm{load}}}=-\left(\frac{1}{K_g+\sum_{i=1}^{n}K_{\mathrm{m}i}(s)}\right) \tag{11}$$

If the VSG's control parameters and port impedances are similar, the system can be approximately analyzed as a single-machine system. In this case, considering the dynamic frequency response of nodes in a multi-machine system has its limitations. Therefore, this paper analyzes a multi-VSG topology that considers the line impedance between nodes.

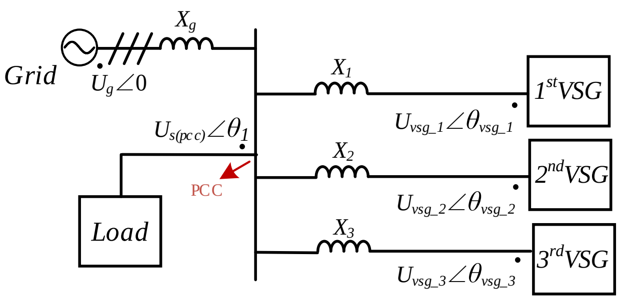

Figure 2. The topology of a single-node three-machine grid-connected system.

3.2. Transfer Function Model of a Multi-Node Multi-Machine Grid-Connected System

To illustrate the general characteristics of frequency response under impedance effects, this paper investigates the transfer function model in a three-node three-VSG grid structure, as shown in Figure 3, to obtain the principle that can be further used in the system with more VSGs. Firstly, due to the presence of line impedance between nodes, spatial differences arise among the nodes. It is necessary to distinguish between each node, the connected VSGs, and the loads. To clearly express the relationships between quantities in a multi-node system, the state variables are defined and represented in vector form.

$$\begin{cases}\Delta\omega_{\mathrm{vsg}}=\begin{bmatrix}\Delta\omega_{\mathrm{vsg\_1}} & \Delta\omega_{\mathrm{vsg\_2}} & \Delta\omega_{\mathrm{vsg\_3}}\end{bmatrix}^{\mathrm{T}}\\ \Delta\theta_{\mathrm{node}}=\begin{bmatrix}\Delta\theta_{\mathrm{node\_1}} & \Delta\theta_{\mathrm{node\_2}} & \Delta\theta_{\mathrm{node\_3}}\end{bmatrix}^{\mathrm{T}}\\ \Delta P_{\mathrm{vsg}}=\begin{bmatrix}\Delta P_{\mathrm{vsg\_1}} & \Delta P_{\mathrm{vsg\_2}} & \Delta P_{\mathrm{vsg\_3}}\end{bmatrix}^{\mathrm{T}}\\ \Delta P_{\mathrm{load}}=\begin{bmatrix}\Delta P_{\mathrm{load\_1}} & \Delta P_{\mathrm{load\_2}} & \Delta P_{\mathrm{load\_3}}\end{bmatrix}^{\mathrm{T}}\end{cases} \tag{12}$$

where θ_{node} is the voltage phase at the node and subscript i is used to distinguish each node, along with the VSG and load connected to it.

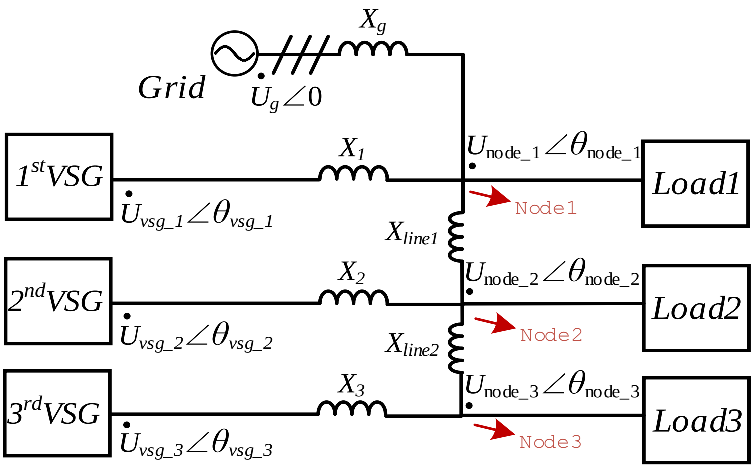

Figure 3. The topology of a three-node three-machine grid-connected system.

Combining the content from Section 2, Equation (13) holds.

$$\Delta P_g + \sum_{i=1}^{3} \Delta P_{\text{vsg}\_i} = \sum_{i=1}^{3} \Delta P_{\text{load}\_i} \tag{13}$$

Considering the relationship of active power between nodes, Equation (14) holds.

$$\frac{3U_{\text{node}\_i} U_{\text{node}\_i+1}}{2X_{\text{line}\_i}} \Delta\delta_{\text{node}\_i} = k_{\text{L}\_i}(\Delta\theta_{\text{node}\_i} - \Delta\theta_{\text{node}\_i+1}) \tag{14}$$

where U_{node} is the voltage at the node; k_{L} is the line coefficient under the assumption of there being no voltage magnitude variation. Considering the power flow relationships in the three-node system, Equation (15) holds.

$$\begin{cases} K_{\text{L}\_1}(\Delta\theta_{\text{node}\_1} - \Delta\theta_{\text{node}\_2}) = \Delta P_{\text{load}\_2} + \Delta P_{\text{load}\_3} - \Delta P_{\text{vsg}\_\text{out}\_2} - \Delta P_{\text{vsg}\_\text{out}\_3} \\ K_{\text{L}\_2}(\Delta\theta_{\text{node}\_2} - \Delta\theta_{\text{node}\_3}) = \Delta P_{\text{load}\_3} - \Delta P_{\text{vsg}\_\text{out}\_3} \end{cases} \tag{15}$$

Combining Equations (5)–(10) and (13)–(15) and expressing them using the vector form in Equation (12), the following relationship holds.

$$\begin{cases} \Delta\omega_{\text{vsg}} = \text{A}_1 \Delta P_{\text{out}} \\ \Delta P_{\text{out}} = \text{A}_2 \Delta\theta_{\text{node}} \\ \text{A}_3 \Delta P_{\text{out}} + \text{A}_4 \Delta\theta_{\text{node}} = \text{A}_5 \Delta P_{\text{load}} \end{cases} \tag{16}$$

where

$$A_2 = \begin{bmatrix} -\dfrac{1}{J_i\omega_0 s + k_{\mathrm{p}\_i}} & 0 & 0 \\ 0 & -\dfrac{1}{J_i\omega_0 s + k_{\mathrm{p}\_i}} & 0 \\ 0 & 0 & -\dfrac{1}{J_i\omega_0 s + k_{\mathrm{p}\_i}} \end{bmatrix}$$

$$A_2 = \begin{bmatrix} -k_{\mathrm{m}\_1}(s) & 0 & 0 \\ 0 & -k_{\mathrm{m}\_2}(s) & 0 \\ 0 & 0 & -k_{\mathrm{m}\_3}(s) \end{bmatrix}$$

$$A_3 = A_5 = \begin{bmatrix} 1 & 1 & 1 \\ 0 & 1 & 1 \\ 0 & 0 & 1 \end{bmatrix}, A_4 = \begin{bmatrix} -k_{\mathrm{g}} & 0 & 0 \\ k_{\mathrm{L}\_1} & -k_{\mathrm{L}\_1} & 0 \\ 0 & k_{\mathrm{L}\_2} & -k_{\mathrm{L}\_2} \end{bmatrix}$$

Performing matrix operations on this equation yields the following result:

$$\Delta\omega_{\mathrm{vsg}} = A_1 A_2 (A_2 A_3 + A_4)^{-1} A_5 \Delta P_{\mathrm{load}} = G\Delta P_{\mathrm{load}} \tag{17}$$

where

$$G = \begin{bmatrix} G_{\omega 11}(s) & G_{\omega 12}(s) & G_{\omega 13}(s) \\ G_{\omega 21}(s) & G_{\omega 22}(s) & G_{\omega 23}(s) \\ G_{\omega 31}(s) & G_{\omega 32}(s) & G_{\omega 33}(s) \end{bmatrix}$$

where G represents the relationship matrix between the frequency of each VSG and the load disturbances. Using this relationship, Equation (18) can be derived.

$$\Delta\omega_{\mathrm{vsg}\_1} = G_{\omega 11}\Delta P_{\mathrm{load}\_1} + G_{\omega 12}\Delta P_{\mathrm{load}\_2} + G_{\omega 13}\Delta P_{\mathrm{load}\_3} \tag{18}$$

And $G_{\omega 1i}$(s) represents the transfer function of the frequency of the *VSG* connected at node 1 with respect to the load power change at node *i*. From Equation (18), it can be observed that in the three-node model, the impact of load disturbances at each node on the frequency of any *VSG* varies. Simplifying these load disturbances as if they all occur at a single node in a single-node model will introduce discrepancies in the dynamic response analysis. The subsequent analysis of the three-node, three-*VSG* model is performed utilizing this transfer function model.

4. Dynamic Frequency Characteristics of Three-Node Three-VSG System

Using the transfer function presented in Section 3, the dynamic frequency responses of each *VSG* can be obtained under load step changes at different nodes. By analyzing the maximum frequency deviation (MFD), rate of change of frequency (RoCoF) and adjustment time to reach a steady state under disturbances, the dynamic characteristics of each *VSG* can be assessed.

This section examines the effects of load disturbance locations, line impedance between nodes, and the virtual inertia (J) and port impedance of each VSG on the frequency dynamic characteristics of VSGs. Sections 4.1 and 4.2 focus on analyzing how variations in practical conditions—such as load disturbance locations and line impedance—affect the dynamic frequency at each node. Conversely, Sections 4.3 and 4.4 investigate how to optimally configure parameters and allocate resources under these varying conditions to achieve an optimized performance in practical scenarios. Specifically, this section identifies the patterns of changes in VSG frequency dynamics influenced by these factors and, based on these observations, proposes and validates optimization strategies for frequency dynamics within a three-node, three-VSG grid.

4.1. Dynamic Frequency Characteristics with Load Disturbances at Different Locations

First, the impact of load disturbance location is analyzed to differentiate between single-node and multi-node models, particularly regarding the consideration of spatial differences between nodes. The findings highlight the comprehensiveness and practicality of multi-node models in capturing dynamic characteristics more effectively compared to single-node models.

The specific parameters are outlined in Table 1. To reflect the differences caused by disturbance location, disturbances are concentrated at each of the three nodes. The frequency characteristics of the VSGs at the initial and terminal nodes are observed to derive the underlying patterns. The results are shown in Figure 4.

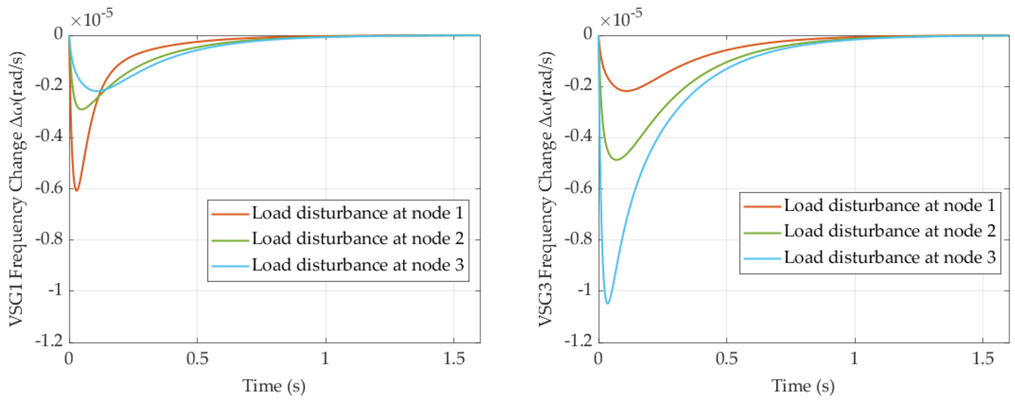

(**a**) VSG1(initial) (**b**) VSG3(terminal)

Figure 4. Step response of VSG frequency at different load positions.

Table 1. Parameter of the transfer function model of three-node three-VSG system.

Parameters	Values
E_{vsg_i} (i = 1, 2, 3)	220 V
U_{node_i} (i = 1, 2, 3)	220 V
J_i	1 kg·m^2
ω_0	314 rad/s
L_g L_i (i = 1, 2, 3)	0.4 mH
L_{XLine_i} (i = 1, 2)	0.4 mH
Kp	50 × 10^3 w·s/rad

For the terminal VSG3, as the disturbance distance increases, the MFD decreases and RoCoF reduces, and the same applies for the initial VSG1. However, the terminal VSG experiences a greater frequency deviation at shorter disturbance distances compared to the initial VSG1, indicating that the dynamic frequency performance of the terminal VSG3 is significantly weaker than that of the initial VSG1. Therefore, to optimize the dynamic frequency characteristics of VSGs in a multi-node model, it is essential to first enhance the dynamic performance of the terminal VSG. Additionally, balancing the load distribution to reduce the burden on the terminal VSG can optimize the overall system's frequency dynamic characteristics.

4.2. Dynamic Frequency Characteristics Under Different Line Impedences

To assess the impact of varying line impedances on the dynamic frequency characteristics of VSGs under load disturbances within this structure, four scenarios are considered in this section. The specific parameters are outlined in Table 2, and other parameters are the same as those listed in Table 1. The results are shown in Figures 5–8.

Scenario 1: The line impedance $L_{\mathrm{Xline\_1}}$ between Nodes 1 and 2 is varied, while the line impedance $L_{\mathrm{Xline\_2}}$ between Nodes 2 and 3 is kept constant. The dynamic frequency responses of the three VSGs are analyzed after the load disturbance is evenly distributed across the three nodes.

Scenario 2: The line impedance $L_{\mathrm{Xline\_1}}$ between Nodes 1 and 2 is varied, while the line impedance $L_{\mathrm{Xline\_2}}$ between Nodes 2 and 3 is kept constant. The dynamic frequency responses of the three VSGs are analyzed following a load disturbance at Node 1.

Scenario 3: The line impedance $L_{\mathrm{Xline\_1}}$ between Nodes 1 and 2 is varied, while the line impedance $L_{\mathrm{Xline\_2}}$ between Nodes 2 and 3 is kept constant. The dynamic frequency responses of the three VSGs are analyzed following a load disturbance at Node 3.

Scenario 4: Both the line impedance $L_{\mathrm{Xline\_1}}$ between Nodes 1 and 2 and the line impedance $L_{\mathrm{Xline\_2}}$ between Nodes 2 and 3 are varied. The dynamic frequency responses of the three VSGs are analyzed following a load disturbance at Node 1.

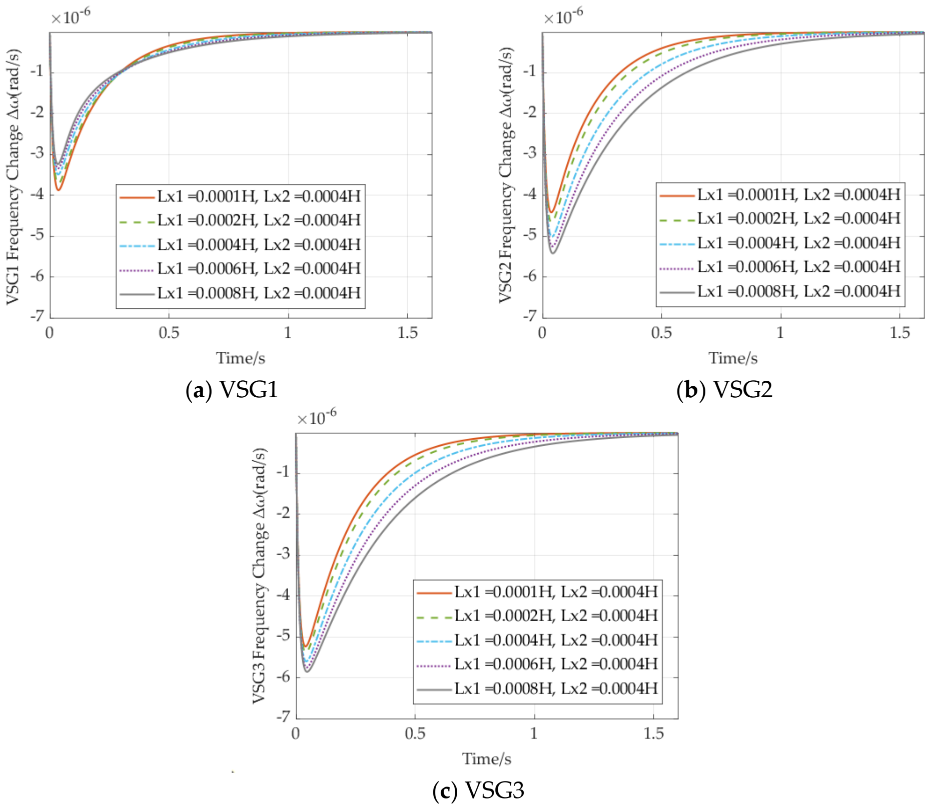

Figure 5. Step response of VSG frequency in scenario 1.

Table 2. Parameter of the transfer function model of the three-node three-VSG system.

Scenario	$L_{\mathrm{Xline\_1}}$ (Lx1)	$L_{\mathrm{Xline\_2}}$ (Lx2)	Load Set
1	0.1/0.2/0.4/0.6/0.8 mH	0.4 mH	Evenly
2	0.1/0.2/0.4/0.6/0.8 mH	0.4 mH	Node 1
3	0.1/0.2/0.4/0.6/0.8 mH	0.4 mH	Node 3
4	0.1/0.2/0.4/0.6/0.8 mH	0.1/0.2/0.4/0.6/0.8 mH	Node 1

As can be observed in Figure 5, when load disturbances are reasonably distributed across each node, increasing the line impedance between Node 1 and Node 2 results in a reduction in the MFD of VSG1, along with an increase in the adjustment time, effectively improving the frequency dynamic response in the microgrid context. However, the MFD of the VSGs connected at Node 2 and Node 3 increases, leading to a certain loss in dynamic performance at those nodes. Furthermore, as shown in Figure 5b,c, both the MFD and RoCoF increase as the VSG is closer to the terminal, demonstrating that the dynamic performance of the frequency deteriorates when the node approaches the end of the line.

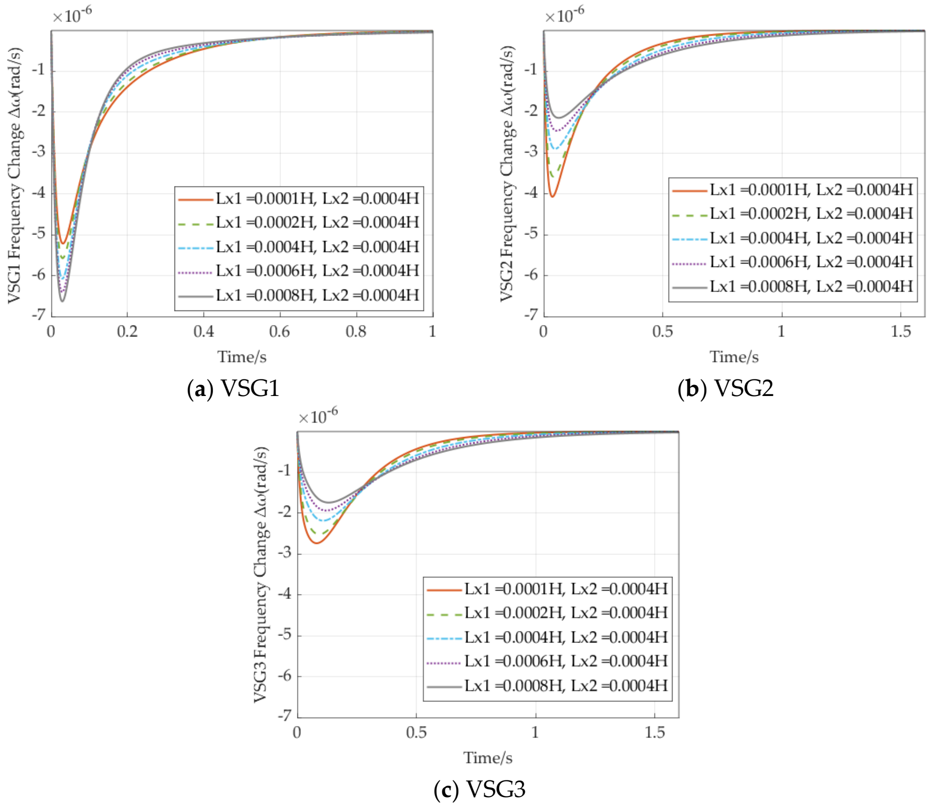

Figure 6. Step response of VSG frequency in scenario 2.

From Figure 6, when load disturbances are primarily concentrated at Node 1 (the initial node), the frequency variation of VSGs closer to Node 1 is larger, indicating that load disturbances primarily rely on local VSGs for inertia support. The impact on VSGs further from the disturbance is smaller. Even at the terminal, where VSG3 is more susceptible to disturbances, the frequency deviation and rate of change are significantly smaller compared to VSG1 and VSG2, which are closer to the initial node. Increasing the line impedance between Node 1 and Node 2 causes load disturbances to rely even more on the inertia support provided by local VSGs. Consequently, the frequency deviation of VSG1 increases, adjustment time decreases, and dynamic performance deteriorates. In contrast, VSGs 2 and 3, separated by the impedance between Nodes 1 and 2, experience a reduction in frequency deviation and rate of change. This suggests that increased line impedance acts as a barrier to disturbances, making local disturbances more reliant on local VSG inertia support and consequently reducing the dynamic frequency characteristics of the local VSG.

When disturbances are concentrated at Node 3 (the terminal) in Figure 7, increasing the line impedance between Node 1 and Node 2 results in a decrease in the dynamic performance of VSG2 and VSG3 at Nodes 2 and 3, while the dynamic performance of VSG1 at Node 1 improves. This demonstrates that line impedance acts as a barrier to load disturbances, with the impact of the disturbances being increasingly supported by VSG2 and VSG3, which are separated by the impedance.

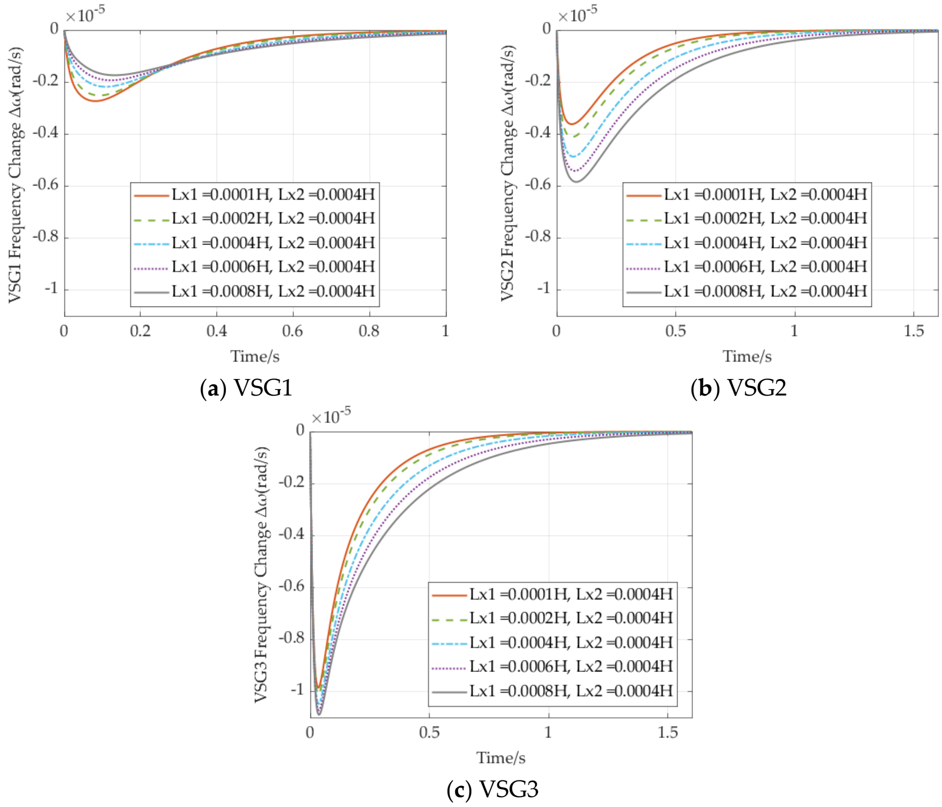

Figure 7. Step response of VSG frequency in scenario 3.

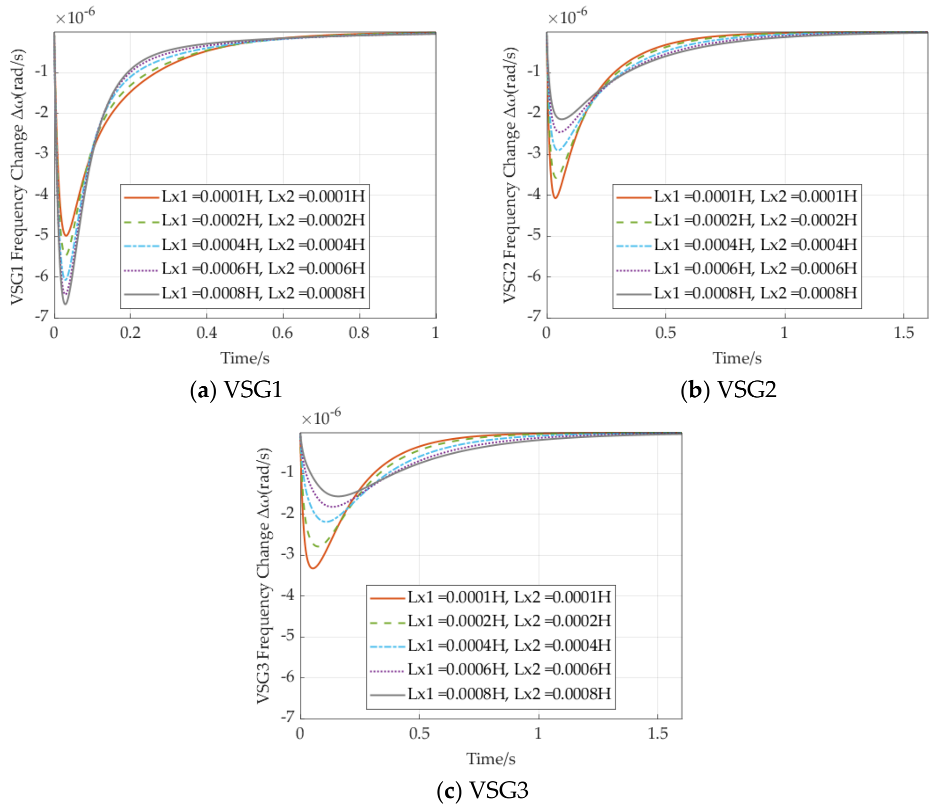

Figure 8. Step response of VSG frequency in scenario 4.

As the line impedance between nodes increases in Figure 8, it further limits the propagation of load disturbances, resulting in greater support for the disturbances from the local VSG1. The impact on VSG2 and VSG3 is reduced, which benefits the optimization of the dynamic frequency characteristics of VSG2 and VSG3.

4.3. Dynamic Frequency Characteristics Under Different Inertia

VSGs require additional capacity to provide virtual inertia, with larger virtual rotational inertia necessitating greater investment. Therefore, optimizing the allocation of virtual inertia is crucial from an economic perspective. In this section, the impact of virtual inertia allocation is analyzed using a three-node, three-VSG model. To evaluate the effect of varying inertia on the dynamic frequency response of VSGs under load disturbances, three scenarios are considered. The parameters are detailed in Table 3, and the results are presented in Figures 9–14.

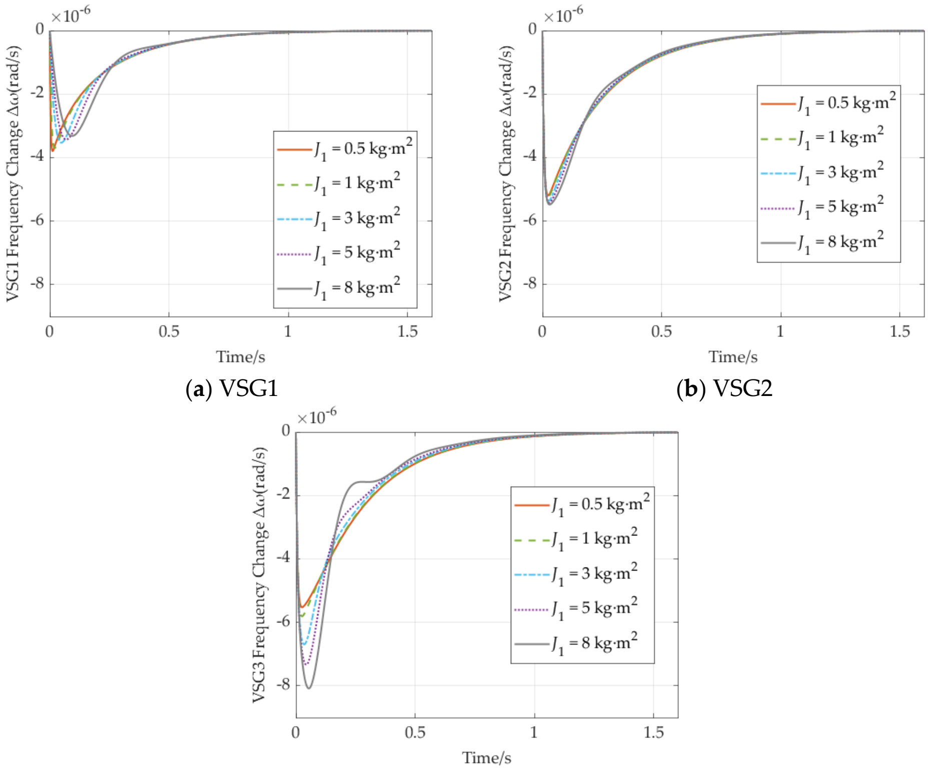

(**a**) VSG1 (**b**) VSG2 (**c**) VSG3

Figure 9. Step response of VSG frequency in scenario 1.

Table 3. Parameter of the transfer function model of three-node three-VSG system.

Scenario	J_1	X_{line_1}/X_{line_2}	Load Set
1	0.5/1/3/5/8 kg·m^2	0.4 mH	Evenly
2	0.5/1/3/5/8 kg·m^2	0.4 mH	Node 1
3	0.5/1/3/5/8 kg·m^2	0.4 mH	Node 3

When load disturbances are evenly distributed across each node and the line impedance between nodes is set to 0.4 mH, the MFD and RoCoF are larger for VSG3, which is closer to the terminal. This further confirms that the dynamic frequency performance of VSGs deteriorates as they approach the terminal. Additionally, as the inertia (J) of the initial VSG1 increases, the dynamic frequency characteristics of VSG1 are optimized, while those of VSG2 and VSG3 deteriorate. Notably, the MFD of VSG3, closer to the terminal, is greater than that of VSG2. This indicates that when load disturbances are evenly distributed, the optimization of dynamic performance at the initial end results in a further improvement in dynamic performance at the terminal end.

Figure 10 shows that when the load is evenly distributed across the three nodes, both the MFD and RoCoF of VSG1 exhibit a decreasing trend as J_1 varies, leading to improved dynamic frequency characteristics. Specifically, the rise in RoCoF, indicating a slower rate of frequency decline, contributes to the optimization of the frequency's dynamic response. In contrast, the MFD of VSG2 and VSG3, positioned at terminal nodes, displays a more substantial variation, with this trend becoming more pronounced as they are located closer to the network's edge.

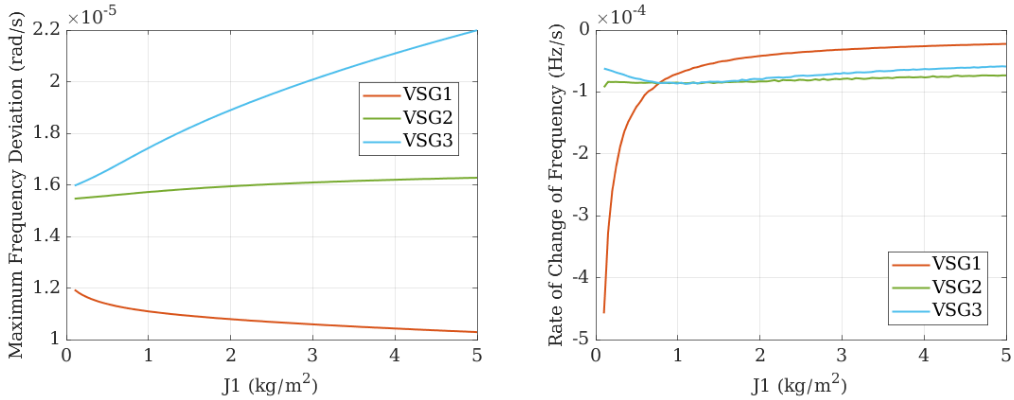

(**a**) MFD (**b**) RoCoF

Figure 10. MFD and RoCoF in scenario 1.

Figure 11 shows that when load disturbances are primarily concentrated at Node 1, increasing the virtual inertia (J) of VSG1 improves its dynamic frequency characteristics. Additionally, this increase also optimizes the dynamic frequency performance of VSG2 and VSG3, which are closer to the terminal. This indicates that when load disturbances are concentrated, increasing the inertia (J) of the local VSG not only enhances the dynamic frequency characteristics of the local VSG but also has a beneficial effect on nearby VSGs.

From Figure 12, it can be clearly observed that as the value of J_1 varies, both the MFD and RoCoF of VSG1 exhibit a more sensitive change compared to VSGs at other nodes, indicating a significant optimization effect. This also demonstrates that the inertia parameter has a greater impact on the local VSG connected to the node where the load disturbance occurs.

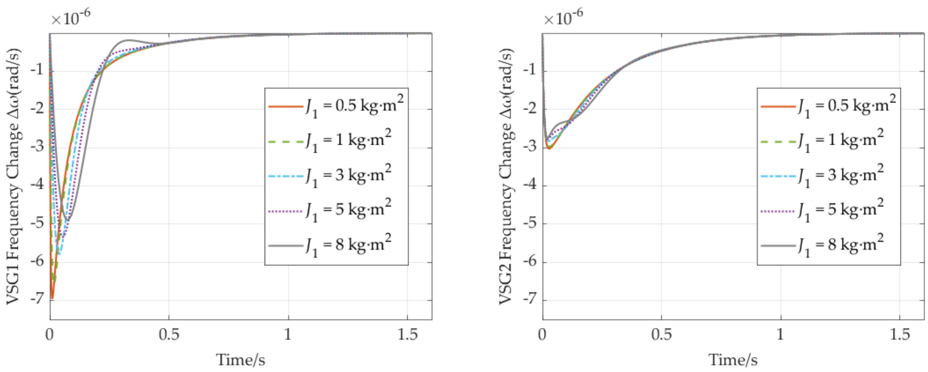

(**a**) VSG1 (**b**) VSG2

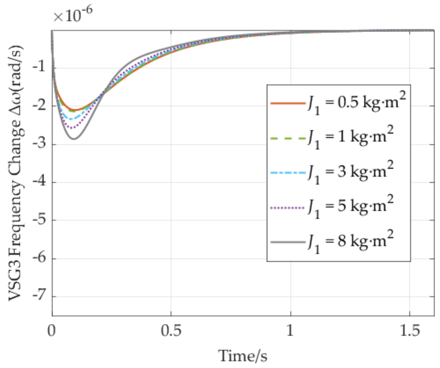

(**c**) VSG3

Figure 11. Step response of VSG frequency in scenario 2.

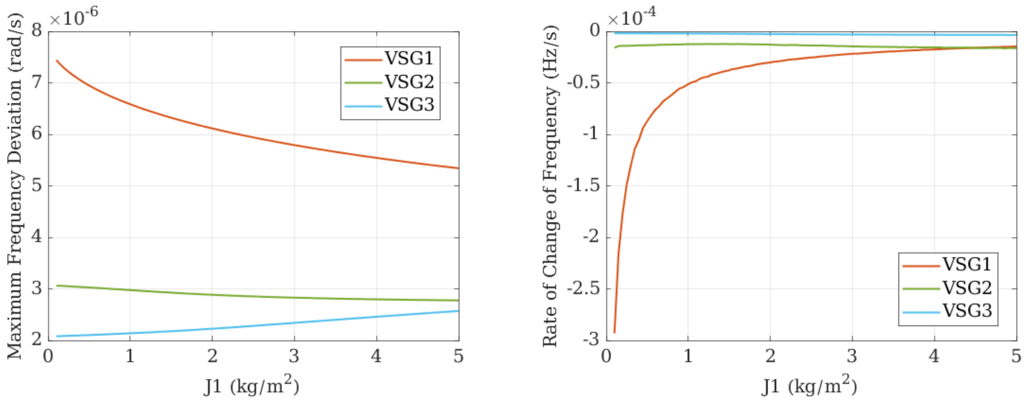

(**a**) MFD (**b**) RoCoF

Figure 12. MFD and RoCoF in scenario 2.

When load disturbances are primarily concentrated at the terminal (Node 3) in Figure 13, increasing the inertia (J) of VSG1 at the initial node results in a decrease in RoCoF but an increase in the maximum frequency deviation of VSG1. The maximum frequency deviation of VSG2 also increases, and the deviation for VSG3 becomes larger compared to VSG2, with increased fluctuations during the recovery process. In this case, increasing the virtual inertia of VSG1 is detrimental to the overall dynamic frequency performance of the system.

From Figure 14, it can be clearly observed that when the load is primarily concentrated at Node 3, the MFD of VSG2 and VSG3 shows a significantly increasing trend as J_1 varies, while VSG1 is not as sensitive. A comparison with Figures 10 and 12 reveals a strong correlation between the setting of inertia (J) and the location where the load is concentrated.

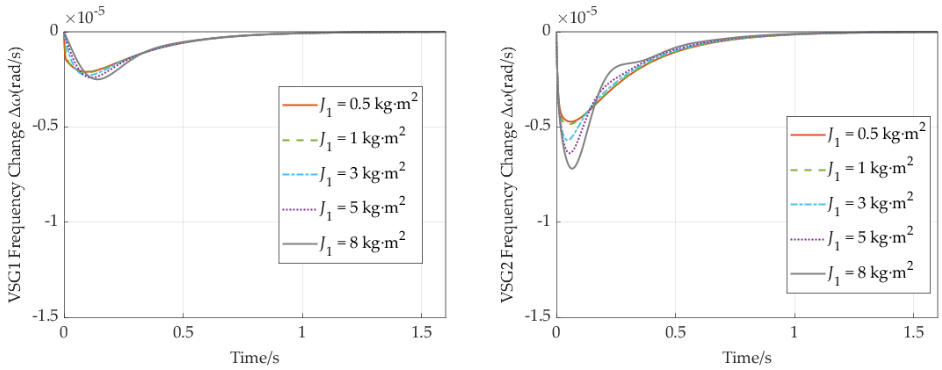

(**a**) VSG1 (**b**) VSG2

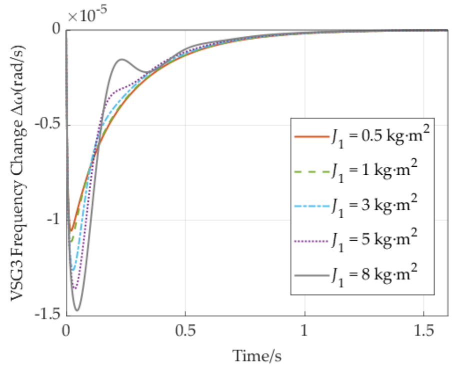

(**c**) VSG3

Figure 13. Step response of VSG frequency in scenario 3.

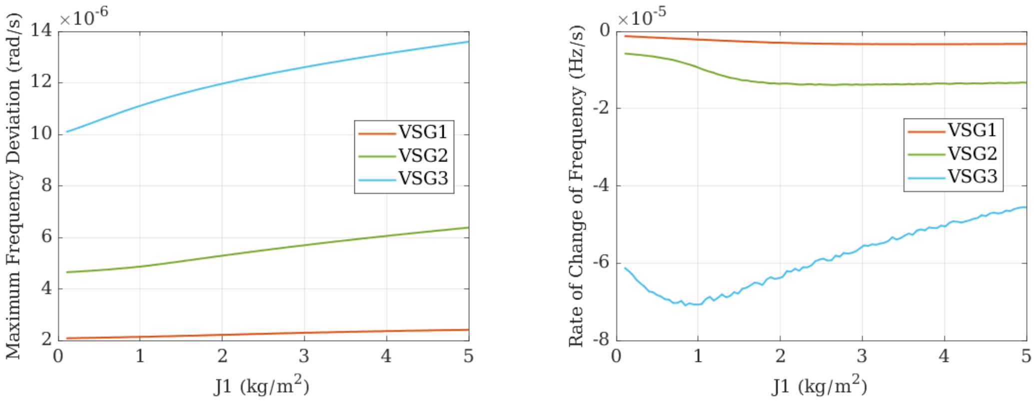

(**a**) MFD (**b**) RoCoF

Figure 14. MFD and RoCoF in scenario 3.

However, it is worth noting that in Figure 10b, as J_1 varies, the RoCoF of VSG3 initially improves and then deteriorates. This indicates that when the inertia parameter is not well matched with the load disturbance, increasing inertia (J) can lead to an overall rise in system MFD, but it also enhances the RoCoF of the VSG at the load location.

4.4. Dynamic Frequency Characteristics Under Different Port Impedances

The output port impedance of the inverter, including line impedance, virtual impedance, and transformer equivalent impedance, can be flexibly adjusted by modifying the virtual impedance. Meanwhile, the line impedance between nodes, as a grid parameter, is generally treated as a fixed value. Thus, studying the impact of VSG port impedance on the frequency dynamic response of the inverter provides another approach to optimizing dynamic performance, which will be discussed in this section.

Considering the conclusion drawn in Section 4.2, when the line impedance between a node and its neighboring nodes decreases, the reliance of the local VSG on frequency support for mitigating local load disturbances is reduced, leading to improved dynamic frequency characteristics for the local VSG, and vice versa. Based on this conclusion, a hypothesis can be proposed: when the impedance at the VSG port increases, the load disturbance at the connected node will reduce its reliance on the frequency support of the corresponding VSG (i.e., the local VSG), thereby improving the local VSG's dynamic frequency characteristics, but at the cost of deteriorating the dynamic frequency performance of other VSGs in the system.

To validate the aforementioned hypothesis and explore the influence of inertia within this context, this section establishes two scenarios for discussion. The specific parameters are outlined in Table 4 and the results are shown in Figures 15–18.

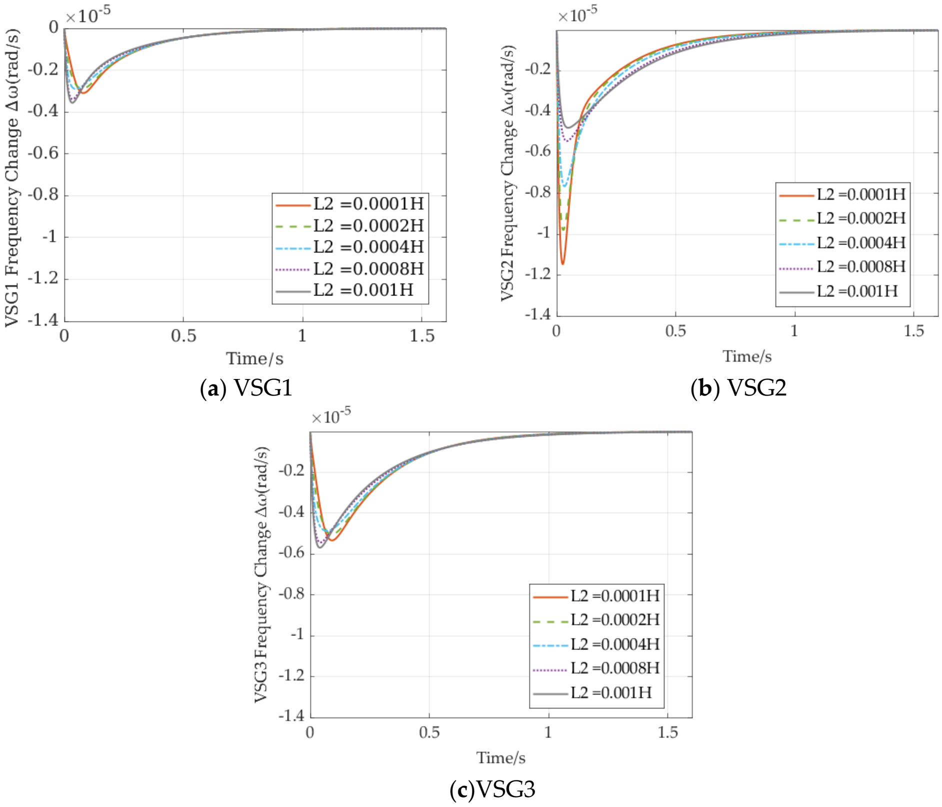

Figure 15. Step response of VSG frequency in scenario 1.

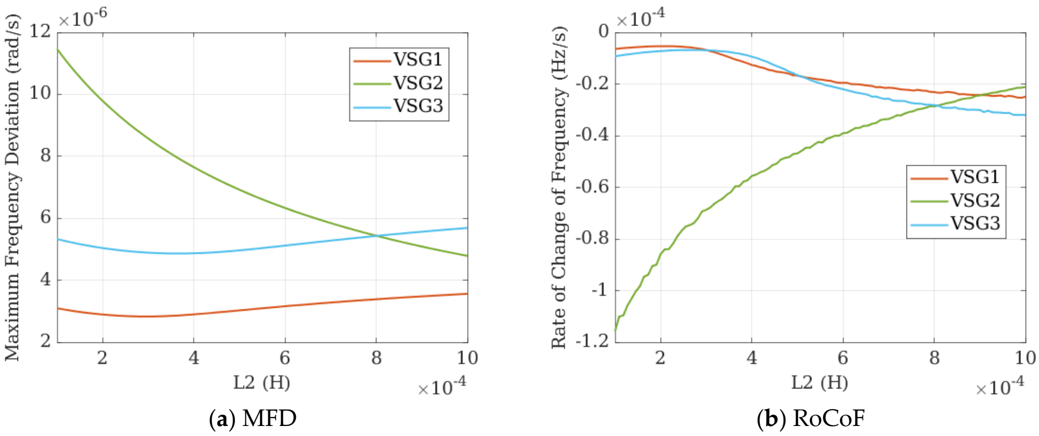

Figure 16. MFD and RoCoF in scenario 1.

Table 4. Parameter of the transfer function model of three-node three-VSG system.

Scenario	$J_1/J_2/J_3$	L_2	Load Set
1	2/2/2 kg·m²	0.1/0.2/0.4/0.8/1 mH	Node 2
2	1/1/1 kg·m²	0.1/0.2/0.4/0.8/1 mH	Node 2

In Figure 15, when the load disturbance is primarily concentrated at Node 2, increasing the port impedance of VSG2 results in a significant reduction in the frequency deviation and an increase in the recovery time of VSG2. This indicates that the dynamic frequency characteristics of VSG2 are optimized as the port impedance increases, thus validating the hypothesis that increasing port impedance benefits the dynamic frequency characteristics of VSGs.

At the same time, the frequency response of neighboring VSGs, VSG1 and VSG3, follows a similar pattern. As the port impedance L2 increases to 1 mH, the frequency deviation range and rate reach their maximum, causing a deterioration in frequency characteristics. When L2 is reduced gradually to 0.2 mH, the frequency deviation decreases and reaches its minimum value. However, further decreasing L2 to 0.1 mH results in an increase in frequency deviation range.

From Figure 16, it can also be observed that as the port impedance L2 increases, both the MFD and RoCoF of VSG2 show a significant improvement trend. However, the frequency responses of the other two VSGs deteriorate correspondingly.

This demonstrates that increasing port impedance can negatively impact the dynamic characteristics of VSGs at other nodes. Additionally, it is observed that the frequency response deviation of VSG3 is notably larger than that of VSG1, corroborating the conclusion in Section 4.1.

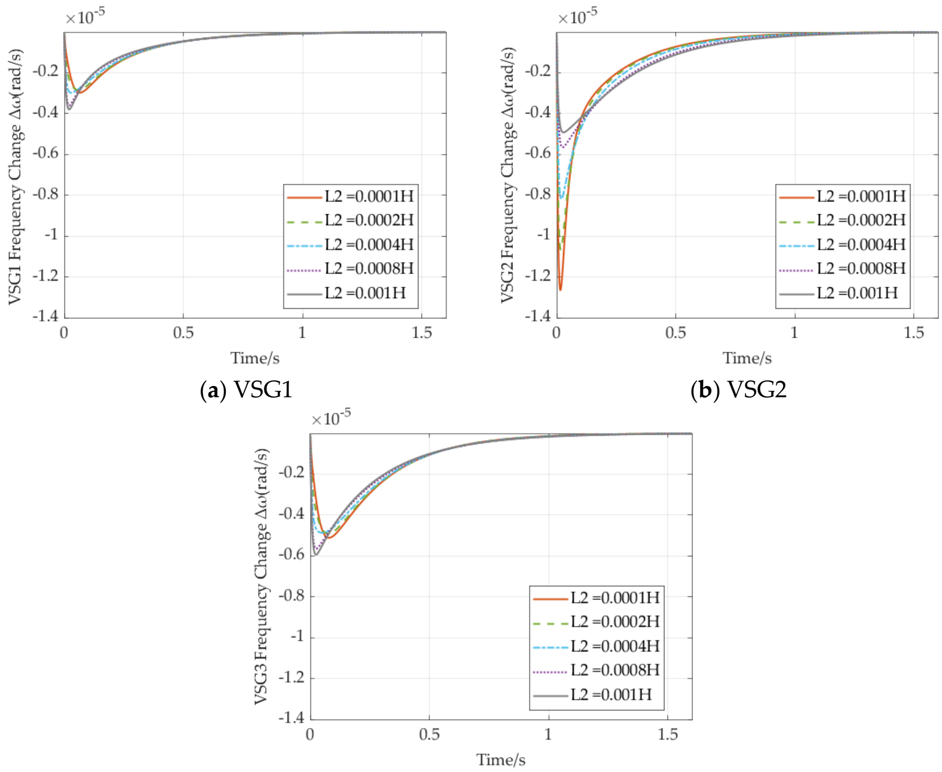

(**a**) VSG1 (**b**) VSG2 (**c**) VSG3

Figure 17. Step response of VSG frequency in scenario 2.

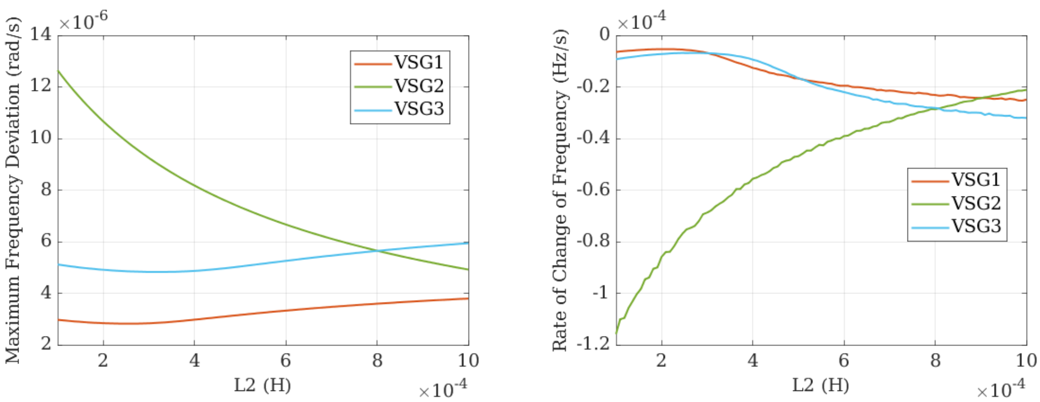

(**a**) MFD (**b**) RoCoF

Figure 18. MFD and RoCoF in scenario 2.

In Case 2, when the virtual inertia (J) of all three VSGs is simultaneously reduced, the frequency response characteristics follow a pattern similar to that observed in Case 1. Specifically, the frequency deviation range of VSG2 increases significantly when the port impedance is small, while the frequency deviations of VSG1 and VSG3 remain relatively unchanged. As the port impedance increases to 1 mH, the frequency deviation range of VSG2 shows minimal variation.

This indicates that as the port impedance decreases, the impact of the virtual inertia set on the VSGs becomes more pronounced compared to when the port impedance is large. Therefore, while considering the efficiency of virtual inertia usage, a larger port impedance for VSGs is not always beneficial. From the comparison between Figures 18 and 16, it can be seen that changing the value of inertia (J) for the three VSGs only affects the magnitude of the values, without impacting the overall trend of variation. Therefore, integrating the conclusions from the above discussion with the experimental results, under the conditions of this section, a port impedance value for L2 in the range of 0.4–0.8 mH is suitable.

4.5. Optimization Strategies and Validation of Dynamic Frequency

From the analysis of the results on the dynamic frequency characteristics of VSGs under various individual and combined influencing factors discussed in Sections 4.1–4.4, the following qualitative conclusions and dynamic performance optimization strategies can be derived:

Sections 4.1 and 4.2 focus on the impact of actual load disturbance locations and line impedance between nodes within the circuit topology on the dynamic frequency characteristics of each VSG. The key qualitative conclusions are as follows:

1. The dynamic frequency characteristics of each VSG vary depending on the location of the load disturbance. The closer the disturbance occurs to the connected node, the greater the MFD and RoCoF during the frequency response process. Additionally, for each VSG, differences arise due to the position of the connected node. Compared to terminal nodes, VSGs located closer to the grid exhibit superior dynamic performance, especially when load disturbances occur at the connected node, where terminal VSGs show poorer performance.

2. Increasing the line impedance between nodes has a detrimental effect on frequency response during unbalanced load conditions. When load disturbances occur at one end of the line impedance, the VSG at the opposite end will participate less in active power regulation during frequency response, thereby improving its dynamic frequency characteristics. Conversely, the dynamic frequency characteristics of the VSG on the load disturbance side will deteriorate.

Sections 4.3 and 4.4 discuss the impact of parameter J and port impedance under specific conditions of node impedance and disturbance locations. The key qualitative conclusions are as follows:

1. When a disturbance occurs at the connected node, increasing the local VSG's inertia can significantly improve its dynamic performance. However, this can lead to a deterioration in the dynamic performance of VSGs at other nodes, with the degree of impact varying depending on the specific location of the disturbance.

2. Increasing the port impedance can improve the dynamic frequency performance of the VSG at the connected node, but it also results in a reduction in performance at other nodes. Increasing the overall system inertia level does not change this trend.

Based on the analysis of the effects of practical influencing factors, as well as the summarized impacts of virtual inertia J and port impedance on the dynamic frequency characteristics of VSGs under different conditions, the following optimization conclusions are derived:

1. The dynamic frequency performance of the VSG at the initial node is better than that at the terminal node. Therefore, optimization should focus on the terminal VSG. The line impedance between connected nodes impedes active power interaction between the two nodes, which in turn worsens the dynamic frequency characteristics on the side where

the load disturbance occurs. Thus, attention should be given to the combined impact of load disturbance location and the magnitude of line impedance between nodes on the dynamic performance at each node, in order to assess the strength of dynamic frequency characteristics for each VSG.

2. The inertia of each VSG should be reasonably set according to the distribution of load disturbances, with increased inertia allocated to areas where load disturbances are concentrated. If the load disturbance does not match the inertia parameter, it is likely to result in a deterioration of the frequency characteristics at the disturbance node, although it may also lead to an improvement in the RoCoF of the VSG at the node connected to the load disturbance.

3. Increasing the port impedance will improve the dynamic frequency characteristics of the VSG at that node, but it will also lead to a deterioration in the dynamic characteristics of VSGs at other nodes. This further necessitates that the port impedance be well matched to the load disturbance location.

To theoretically validate the correctness of the optimization strategies, a set of parameters for the three-node model is considered. Under the guidance of the dynamic frequency optimization strategies, optimization is performed, and the dynamic frequency characteristics of the initial and terminal VSGs are compared before and after the optimization. The parameters before and after optimization are shown in Table 5. And the results are shown in Figure 14.

Table 5. Parameters before and after adjustment.

Fixed Parameters		Values	
L_{xLine_i} (i = 1, 2)		0.4 mH/0.2 mH	
Adjustment	**J1/J2/J3**	**L1/L2/L3**	**Load Set**
Before	3/1/1 kg·m^2	0.4/0.6/0.2 mH	10 kw in Node 3
After	1/1/3 kg·m^2	0.2/0.4/0.6 mH	10 kw in Node 3

From Figure 19, it can be observed that when the load disturbance occurs at the end, specifically at Node 3, increasing the port impedance and virtual inertia at VSG3, while reducing the port impedance of VSG2 and VSG1, effectively optimizes the dynamic frequency response of VSG3. Furthermore, the dynamic frequency response of VSG1, located at the front end, shows no significant changes, demonstrating the effectiveness of this optimization strategy.

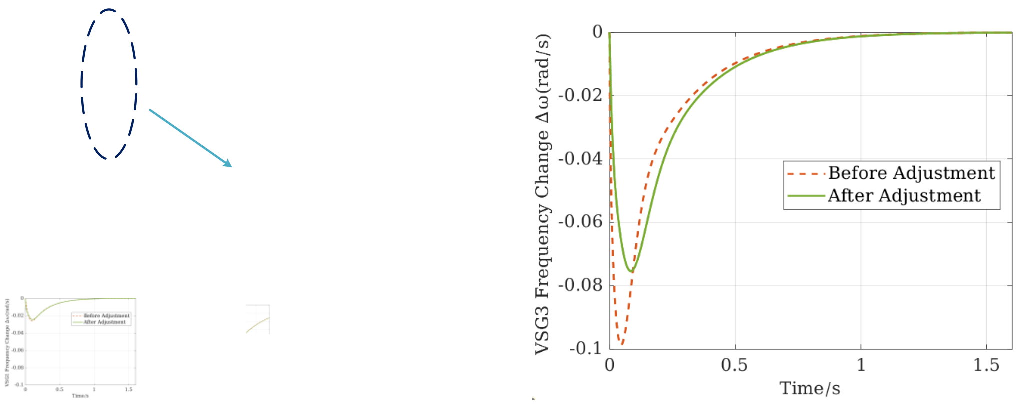

(**a**) VSG1 (**b**) VSG3

Figure 19. Step response of VSG frequency before and after adjustment.

5. Simulation Validation

To further verify the validity of the model and the correctness of the frequency dynamic performance optimization strategy, the topology described in this paper is simulated using PSCAD v46. The simulation model uses the circuit structure shown in Figure 3.

5.1. Validation of the Transfer Function Model

In a three-node three-VSG system, when an external load undergoes a step change at Node 1, the frequency response of three VSGs is shown in Figure 15. And the parameters of the simulation and theoretical experiment are shown in Table 6. It should be noted that in the simulation, to eliminate the influence of inner loop parameters on the dynamic frequency response of each VSG, the inner loop parameters are set to the same values.

Table 6. Parameter of three-node three-VSG system.

Parameters	Values
E_{vsg_i} (i = 1, 2, 3)	220 V
U_{node_i} (i = 1, 2, 3)	220 V
J_i (i = 1, 2, 3)	1 kg m^2
ω_0	314.15 rad/s
Lg L_i (i = 1, 2, 3)	0.4 mH
L_{XLine_i} (i = 1, 2)	0.4 mH
Lf/Cf	2 mH/40 µF
Kp	50 × 10^3 w s/rad
ΔP_{load}	300 kW
Voltage Loop P/I	50/2
Current Loop P/I	0.13/2

As shown in Figure 20, under the same parameter settings and disturbance values, the simulation and theoretical frequency response results exhibit a similar trend, though there is a certain degree of numerical error. This discrepancy is due to the theoretical calculation neglecting the variation in voltage amplitude at the nodes. The oscillations in frequency during the recovery process are determined by the bandwidth difference of the VSG P control loop and the dual-loop bandwidth in the simulation, but this does not affect the correctness of the trend observed in both results. Therefore, it can be concluded that the theoretical model has been validated.

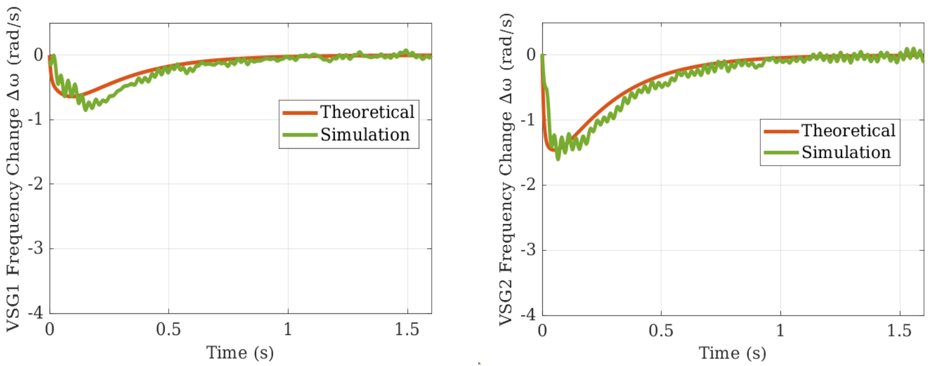

(**a**) VSG1 (**b**) VSG2

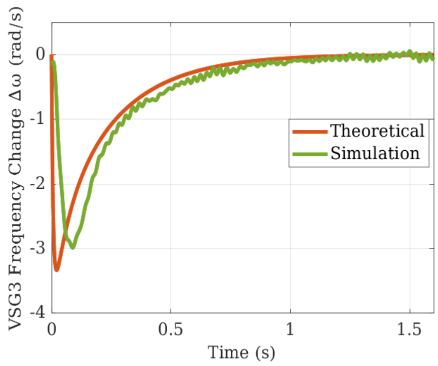

(**c**) VSG3

Figure 20. Theoretical and PSCAD/EMTDC results.

5.2. Validation of the Dynamic Performance Optimization Strategy

Next, the simulation model is used to validate the optimization strategy discussed in Section 4.5, with the specific parameters selected being the same as those in Table 4. And the load disturbance is set as 300 kW. To clearly demonstrate the correctness of the strategy, the results are also validated by analyzing the changes in the VSG port impedance and virtual inertia to eliminate the impact caused by the overlap of the two factors. The specific experimental parameters are shown in Table 7.

Table 7. The simulation experiment parameters.

Scenario	Attribute	J1/J2/J3	L1/L2/L3
1	Reference	3/1/1 kg m^2	0.4/0.6/0.2 mH
2	Vary L	3/1/1 kg m^2	0.2/0.4/0.6 mH
3	Vary J	1/1/3 kg m^2	0.4/0.6/0.2 mH
4	Vary Both	1/1/3 kg m^2	0.2/0.4/0.6 mH

In Figure 21, with only the port impedance changed, both the MFD and RoCoF of VSG3 are significantly improved, while the RoCoF of VSG1 shows a slight reduction. However, the MFD remains similar, and the overall system dynamic frequency performance is enhanced. This indicates that the adjustment of variable port impedance has effectively optimized the frequency dynamic response.

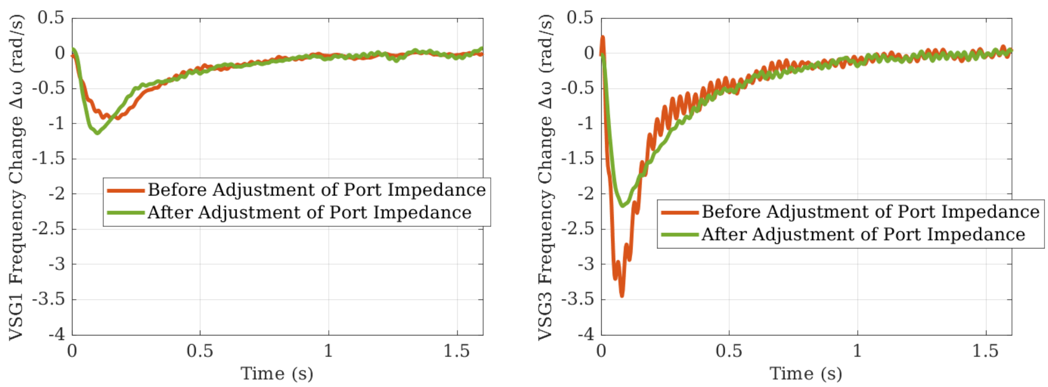

(**a**) VSG1 (**b**) VSG3

Figure 21. Simulation validation results of varying port impedance.

In Figure 22, similarly, when only the inertia is changed without altering the port impedance, the RoCoF of VSG3 decreases, but the MFD of VSG3 shows little variation. Meanwhile, the RoCoF of VSG1, located at the initial end, remains nearly constant.

Although the overall system dynamic frequency performance improves, the effect is not pronounced, which indicates that when the port impedance is not optimally configured, the frequency optimization benefits from increased inertia are limited.

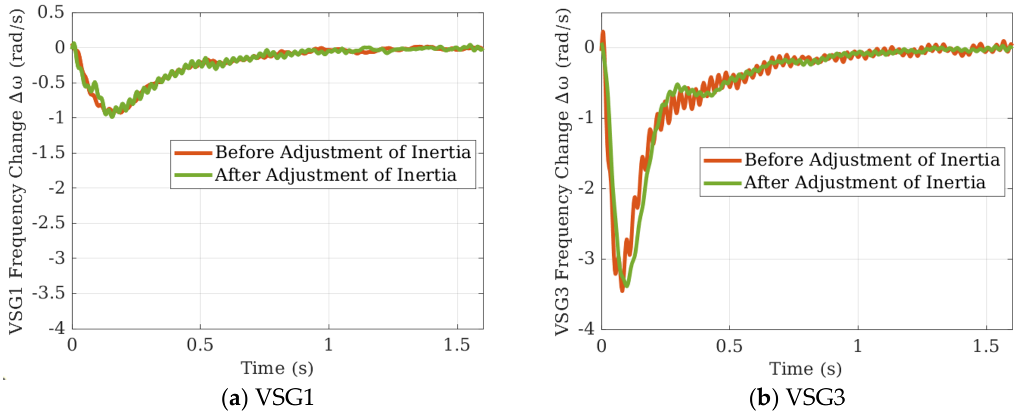

Figure 22. Simulation validation results of varying inertia..

In Figure 23, when both factors are altered, the dynamic performance of VSG3 shows significant improvement, while the RoCoF of VSG1 increases further, although the MFD remains relatively stable. This indicates a certain degree of enhancement in the system's frequency characteristics, thereby demonstrating the effectiveness of the frequency optimization strategy. And the specific experimental results are shown in the tables below.

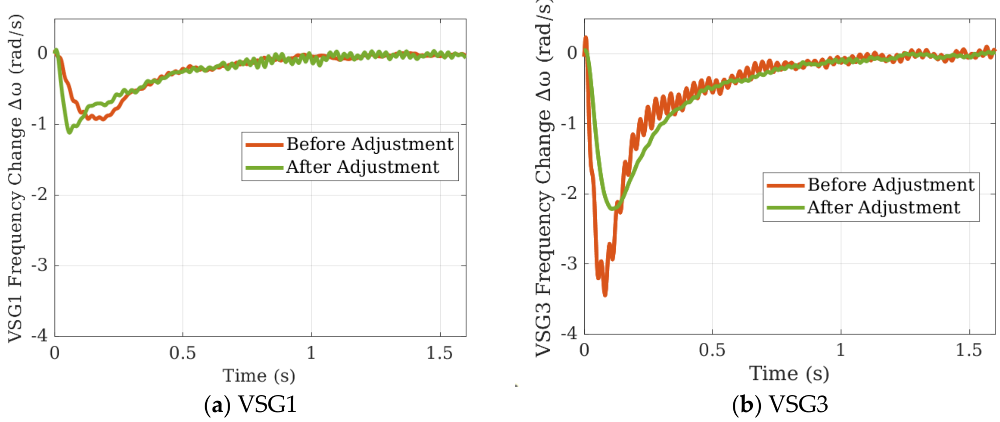

Figure 23. Simulation validation results of varying both factors.

Table 8 presents the MFD and RoCoF of each VSG during the frequency response process under each experimental condition, along with percentage comparisons to the reference group. From Table 8, a comparison between groups 1 and 4 clearly shows that under the dynamic frequency optimization strategy proposed in this paper, the MFD of the terminal VSG3 at the disturbance location significantly decreases, reaching only 62% of its value before adjustment. Although the MFDs of VSG1 and VSG2 both increase, Table 9 shows that the system's average MFD is only 86.1% of the original, demonstrating the effectiveness of the optimization strategy.

Table 8. The first set of specific experimental results.

Scenario	VSG1		VSG2		VSG3	
	MFD (rad/s)	RoCoF (Hz/s)	MFD (rad/s)	RoCoF (Hz/s)	MFD (rad/s)	RoCoF (Hz/s)
1 (Reference)	0.788777	−0.154971	1.279293	−0.210996	3.069388	−0.158310
2	0.937706	−0.128584	1.517007	−0.053582	1.973153	−0.138003
	1.19 × 100%	1.17 × 100%	1.19 × 100%	1.75 × 100%	0.64 × 100%	0.87 × 100%
3	0.908160	−0.159783	1.411547	−0.274579	2.723192	−0.325253
	1.15 × 100%	1.03 × 100%	1.10 × 100%	1.30 × 100%	0.89 × 100%	2.06 × 100%
4	0.896958	−0.189921	1.618510	−0.082723	1.908000	−0.240437
	1.14 × 100%	1.23 × 100%	1.27 × 100%	1.61 × 100%	0.62 × 100%	1.52 × 100%

Table 9. The second set of specific experimental results.

Scenario	Average of Three VSGs	
	MFD (rad/s)	RoCoF (Hz/s)
1 (Reference)	1.712486	−0.174759
2	1.475289	−0.106723
	0.861 × 100%	0.611 × 100%
3	1.680300	−0.253205
	0.981 × 100%	1.449 × 100%
4	1.474489	−0.171027
	0.861 × 100%	0.979 × 100%

However, it is noteworthy that the comparison between scenarios 2 and 4 in Table 9 reveals that, despite similar average MFDs, reducing J1 and increasing J3 leads to a deterioration in the system's average RoCoF. The data in Table 8 indicate that the RoCoF change of the terminal VSG3 is most pronounced, consistent with the trend shown in Figure 14b in Section 4.3. This also highlights that when considering inertia configuration, it is insufficient to match the inertia only to the load; the impact of inertia reduction at non-disturbance nodes on the RoCoF at the disturbance node must also be considered.

Overall, the frequency optimization strategy proposed in this paper proves to be effective.

6. Conclusions

Considering a practical microgrid structure, this paper proposes a multi-node, multi-machine model that takes into account the line impedance between nodes and establishes a transfer function model from load disturbances to VSG frequency response. By analyzing the impact of inter-node line impedance and load disturbance location on dynamic frequency, as well as studying the effects of configuring parameters such as virtual inertia and port impedance under different disturbance conditions, a strategy is ultimately proposed to improve the dynamic frequency response of VSGs in multi-node microgrids. This approach explicitly considers spatial differences between nodes and provides a more effective strategy for improving frequency response in multi-node microgrid systems. The main conclusions are as follows:

1. Compared with traditional single-node analysis methods, the proposed strategy significantly enhances the dynamic frequency characteristics of the system under different load disturbance conditions. By appropriately adjusting virtual inertia and port impedance, the MFD and RoCoF of the system are effectively reduced, resulting in greater resistance to frequency disturbances.

2. The proposed method is suitable for complex, practical microgrid systems, taking into account the effects of inter-node line impedance and spatial differences, which improves the consistency of frequency response. At the same time, the strategy improves resource utilization efficiency and reduces the need for over-dimensioned hardware,

although it also increases the complexity of modeling and parameter tuning, which may pose challenges for simpler systems.

Future research will focus on addressing the issue that optimizing frequency characteristics at specific nodes may lead to reduced performance at other nodes, in order to achieve balanced frequency response across all nodes. In addition, more advanced optimization algorithms will be explored to achieve deeper performance improvements, ultimately enabling optimal control solutions.

Author Contributions: Conceptualization, L.L.; Methodology, W.X. and W.K.; Software, Z.P.; Validation, X.L.; Formal analysis, W.X.; Resources, D.J.; Writing—original draft, W.X.; Writing—review & editing, D.J. and C.X.; Visualization, Z.Y. All authors have read and agreed to the published version of the manuscript.

Funding: The results of this paper is based on the project JYEPJS20230253 (Research of VSG for energy storage).

Data Availability Statement: The original contributions presented in the study are included in the article, further inquiries can be directed to the corresponding author.

Conflicts of Interest: Authors Wei Xie, Liangzi Li, Weihao Kong, Zheng Peng, Xiaogang Li and Dandan Jiao were employed by Henan Jiuyu Enpai Power Technol Co., Ltd. The remaining authors declare that the research was conducted in the absence of any commercial or financial relationships that could be construed as a potential conflict of interest.

References

1. Tian, J.; Wang, F.; Zhuo, F.; Wang, Y.; Wang, H.; Li, Y. A zero-backflow-power EPS control scheme with multiobjective coupled-relationship optimization in DAB-based converter. *IEEE J. Emerg. Sel. Top. Power Electron.* **2021**, *10*, 4128–4145.
2. Zhu, Z.; Sun, S.; Huang, S. ILADRC resonance suppression control strategy for multiple parallel photovoltaic energy storage GFL VSG microgrid. *Electr. Eng.* **2024**, 1–14.
3. Guan, M.; Pan, W.; Zhang, J.; Hao, Q.; Cheng, J.; Zheng, X. Synchronous generator emulation control strategy for voltage source converter (VSC) stations. *IEEE Trans. Power Syst.* **2015**, *30*, 3093–3101.
4. Li, Y.; Gu, Y.; Green, T.C. Revisiting grid-forming and grid-following inverters: A duality theory. *IEEE Trans. Power Syst.* **2022**, *37*, 4541–4554.
5. Wang, Z.; Yi, H.; Zhuo, F.; Sun, L.; Pei, Y.; Zhai, H.; Wu, J. A hardware structure of virtual synchronous generator in photovoltaic microgrid and its dynamic performance analysis. *Proc. CSEE* **2017**, *37*, 444–453.
6. Liu, J.; Miura, Y.; Ise, T. Comparison of dynamic characteristics between virtual synchronous generator and droop control in inverter-based distributed generators. *IEEE Trans. Power Electron.* **2015**, *31*, 3600–3611.
7. Torres, M.; Lopes, L.A. Virtual synchronous generator control in autonomous wind-diesel power systems. In Proceedings of the 2009 IEEE Electrical Power & Energy Conference (EPEC), Montreal, QC, Canada, 22–23 October 2009; pp. 1–6.
8. Hu, B.; Cao, W.; Yang, M.; Lu, Y. The Optimal Ratio of GFM-Converters to GFL-Converters for Transient Voltage Regulation with Weak Grid Condition. In Proceedings of the 2023 IEEE 7th Conference on Energy Internet and Energy System Integration (EI2), Hangzhou, China, 15–18 December 2023; pp. 1993–1998.
9. Zhou, S.; Zou, X.; Zhu, D.; Tong, L.; Zhao, Y.; Kang, Y.; Yuan, X. An improved design of current controller for LCL-type grid-connected converter to reduce negative effect of PLL in weak grid. *IEEE J. Emerg. Sel. Top. Power Electron.* **2017**, *6*, 648–663.
10. Askarian, A.; Park, J.; Salapaka, S. Enhanced Grid Following Inverter (E-GFL): A Unified Control Framework for Stiff and Weak Grids. *IEEE Trans. Power Electron.***2024**, *39*, 5089–5107.
11. Alipoor, J.; Miura, Y.; Ise, T. Stability assessment and optimization methods for microgrid with multiple VSG units. *IEEE Trans. Smart Grid* **2016**, *9*, 1462–1471.
12. Driesen, J.; Visscher, K. Virtual synchronous generators. In Proceedings of the 2008 IEEE Power and Energy Society General Meeting-Conversion and Delivery of Electrical Energy in the 21st Century, Pittsburgh, PA, USA, 20–24 July 2008; pp. 1–3.
13. Sakimoto, K.; Miura, Y.; Ise, T. Stabilization of a power system including inverter-type distributed generators by a virtual synchronous generator. *Electr. Eng. Jpn.* **2014**, *187*, 7–17.
14. Chen, Y.; Hesse, R.; Turschner, D.; Beck, H.P. Improving the grid power quality using virtual synchronous machines. In Proceedings of the 2011 International Conference on Power Engineering. Energy and Electrical Drives, Malaga, Spain, 11–13 May 2011, pp. 1–6.
15. Bevrani, H.; Ise, T.; Miura, Y. Virtual synchronous generators: A survey and new perspectives. *Int. J. Electr. Power Energy Syst.* **2014**, *54*, 244–254.
16. Rongliang, S.; Xing, Z.; Fang, L.; Haizhen, X.; Yong, Y. Control technologies of multi-energy complementary microgrid operation based on virtual synchronous generator. *Trans. China Electrotech. Soc.* **2016**, *31*, 170–180.

17. Xie, N.; Liu, J.; Wang, Y.; Yin, Z.; Chen, C.; Zhao, Y. Combination analysis of VSG control converter and other converters. In Proceedings of the 2024 3rd International Conference on Energy Power and Electrical Technology (ICEPET), Chengdu, China, 17–19 May 2024; pp. 1868–1875.
18. Wang, G.; Fu, L.; Hu, Q.; Ma, F.; Liu, C.; Lin, Y. Low frequency oscillation analysis of VSG grid-connected system. In Proceedings of the 2021 3rd Asia Energy and Electrical Engineering Symposium (AEEES), Chengdu, China, 26–29 March 2021; pp. 631–637.
19. Sun, D.; Liu, H.; Wu, L.; Song, P.; Wang, X.; Li, D. Modeling and Characteristic Analysis of Influence of Virtual Synchronous Generatoron Low Frequency Oscillation. *Autom. Electr. Power Syst.* **2020**, *44*, 134–144.
20. Li, D.; Zhu, Q.; Lin, S.; Bian, X.Y. A self-adaptive inertia and damping combination control of VSG to support frequency stability. *IEEE Trans. Energy Convers.* **2016**, *2*, 397–398.
21. Qi, Y.; Wu, H.; Pei, X.; Yang, R.; Zheng, Y. A Bandwidth-orienting Simplified and Design Method for Multiple VSG Parallel System. In Proceedings of the 2024 9th Asia Conference on Power and Electrical Engineering (ACPEE), Shanghai, China, 11–13 April 2024; pp. 2624–2629.
22. Choopani, M.; Hosseinian, S.H.; Vahidi, B. New transient stability and LVRT improvement of multi-VSG grids using the frequency of the center of inertia. *IEEE Trans. Power Syst.* **2019**, *35*, 527–538.
23. Zhang, B.; Yan, X.; Huang, Y. Stability control and inertia matching method of multi-parallel virtual synchronous generators. *Trans. China Electrotech. Soc.* **2017**, *32*, 42–52.
24. Rasool, A.; Yan, X.; Rasool, H.; Guo, H. Correlation between multiple VSG sources for enhancing the power allocation in microgrid. In Proceedings of the 2018 IEEE Electrical Power and Energy Conference (EPEC), Toronto, ON, Canada, 10-11 October 2018; pp. 1–6.
25. Fu, S.; Sun, Y.; Li, L.; Liu, Z.; Han, H.; Su, M. Power oscillation suppression in multi-VSG grid by adaptive virtual impedance control. *IEEE Syst. J.* **2022**, *16*, 4744–4755.
26. Wang, W.; Jiang, L.; Cao, Y.; Li, Y. A parameter alternating VSG controller of VSC-MTDC systems for low frequency oscillation damping. *IEEE Trans. Power Syst.* **2020**, *35*, 4609–4621.
27. Wang, Z.; Zhuo, F.; Yi, H.; Wu, J.; Wang, F.; Zeng, Z. Analysis of Dynamic Frequency Performance Among Voltage-Controlled Inverters Considering Virtual Inertia Interaction in Microgrid. *IEEE Trans. Ind. Appl.* **2019**, *55*, 4135–4144. https://doi.org/10.1109/TIA.2019.2910784.
28. Sun, P.; Yao, J.; Zhao, Y.; Fang, X.; Cao, J. Stability Assessment and Damping Optimization Control of Multiple Grid-connected Virtual Synchronous Generators. *IEEE Trans. Energy Convers.* **2021**, *36*, 3555–3567. https://doi.org/10.1109/TEC.2021.3104348.
29. Wang, Z.; Yi, H.; Zhuo, F.; Wu, J.; Zhu, C. Analysis of Parameter Influence on Transient Active Power Circulation Among Different Generation Units in Microgrid. *IEEE Trans. Ind. Electron.* **2020**, *68*, 248–257. https://doi.org/10.1109/TIE.2019.2962447.
30. Chen, M.; Zhou, D.; Wu, C.; Blaabjerg, F. Characteristics of Parallel Inverters Applying Virtual Synchronous Generator Control. *IEEE Trans. Smart Grid* **2021**, *12*, 4690–4701. https://doi.org/10.1109/TSG.2021.3102994.